Journal of Structural Geology, Vol. 12, No. 7, pp. 911 to 921, 1990
Printed in Great Britain

0191-8141/90 $03.00 + 0.00
© 1990 Pergamon Press plc

The control of deformation intensity around a fault: natural and experimental examples

F. ODONNE

Laboratoire de Géologie Structurale et Tectonophysique, Université Paul Sabatier, 38 rue des 36 Ponts, 31400 Toulouse, France

(*Received* 26 *June* 1989; *accepted in revised form* 8 *February* 1990)

Abstract—The deformation intensity around a wrench fault is studied through a comparison between a well-known natural fault and experimental models. Each model consists of a horizontal paraffin wax layer, containing a precut plane, which was submitted to uniaxial compression. The Meyrueis Fault, in the Jurassic formations of the Causses massif (southern French Massif Central) gives the opportunity of estimating strain around a wrench fault. The comparison of this fault with the experimental models shows a good similarity in relation to the following aspects: variation of the principal strain axes around the fault; rotation of the strain axes with time, which confirms a non-coaxial strain history; heterogeneity of strain with some domains strongly deformed and others protected; symmetry of these domains with respect to the fault; and the strong influence of kinematic boundary conditions in the direction perpendicular to the compression. These features provide new criteria for the interpretation of natural wrench faults.

INTRODUCTION

WRENCH faults are well-known structures all over the Earth's surface. They have been observed associated with folds (Freund 1965, Harding 1974) or with second-order fractures and folds (Moody & Hill 1956, Moody 1973). But although faulting is the result of stresses (Coulomb 1776, Oertel 1965, Naylor *et al.* 1986), a fault is not an inactive object, and since Anderson (1951) the reorientation of stresses around faults is well known (Segall & Pollard 1980, Gamond 1983, Xiaohan 1983). Also, a fault, once it exists, may be active over a long period, and the conditions that produce movement along an existing fault are different from conditions that produced the faulting itself (Chinnery 1963, White *et al.* 1986).

The geometry of the deformation that occurs around a wrench fault is also well established (Freund 1970, Wilcox *et al.* 1973). The study of this geometry seems to be only possible in three dimensions (Chinnery 1961, Sanderson & Marchini 1984). However the relationship between the finite strain ellipsoid and the velocity field around a fault is not a straightforward one (McKenzie & Jackson 1983). The purpose of this paper is to explore this domain and to estimate the degree of heterogeneity introduced by a fracture in the deformation of a sedimentary block by a comparison between a well known field example and experimental models.

The Meyrueis Fault, on the Causse Méjean in the southern French Massif Central, is a strike-slip fault with a displacement of a few kilometres (Gèze 1977). This is compared with an analogue model, where a layer of paraffin wax represents the sedimentary cover and a slit made in it represents the fault. Here, the number of situations is multiplied at will by the experimenter, but a model is only an explanation of the reality and not the reality itself. So a discussion is necessary to compare the results of the two examples before attempting to draw any conclusions.

THE MEYRUEIS FAULT, EASTERN CAUSSE MEJEAN

The morphology of the "Causses Majeurs" area, in the southern French Massif Central (Fig. 1), is that of a table-land. Rivers cut the plateau and form deep, narrow valleys known as the gorges of the Tarn. These valleys enable us to observe the structures. East of the Causses, crystalline basement appears, but the Causses themselves are made of Jurassic sedimentary rocks, mainly carbonates. Large faults have cut the region up into blocks, without changing the horizontal attitude of the stratification. Despite this apparent uniformity, small-scale conjugate wrench faults, horizontal tectonic stylolites (Arthaud & Mattauer 1969) and slickolites (Means 1987) on the surfaces of joints and veins are obvious proofs of deformation everywhere on the Causses. In a few places there are some folds (de Charpal & Trémolières 1974), always on a modest scale but clearly defined, and they are commonly close folds. Alphine orogenesis produced faulting and surrounding strain (Chiron 1980).

On the east side of Causse Méjean is the Meyrueis Fault, orientated 030°, well-known for an important left-lateral movement, associated with a lowering of all the western blocks and a thickening by small reverse faults in the eastern blocks (around Florac). To be more precise, the thickness of the sedimentary cover is 1000 m and the western blocks have dropped 200 m. The Meyrueis Fault is in fact a bundle of many individual faults (Fig. 1), but a main fault exists and in this paper it is treated as the only significant one. If faulting is the result of brittle failure, the abundance of stylolites, slickolites

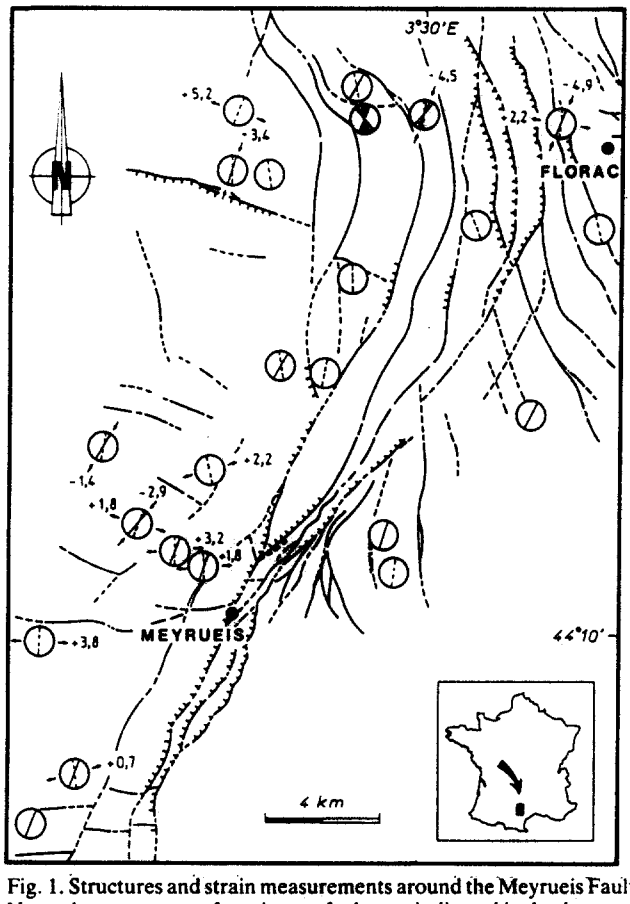

Fig. 1. Structures and strain measurements around the Meyrueis Fault. Normal components of motion on faults are indicated by hachures on the downthrown side. For each point of strain measurement, represented by a small circle, the direction of the veins is represented by a dotted line and the shortening direction is represented by a continuous line. Where the values of extension are known, they are indicated with positive percentages and centrifugal arrows for positive extensions, and negative percentages and centripetal arrows for negative extensions.

and veins suggests that the deformation mechanism involved around the fault is pressure solution.

Wherever deformation has occurred, a strain ellipsoid has resulted. Unfortunately the lack of good strain markers on the Causse means that the exact shapes of these ellipsoids are not known. Nevertheless it is possible to define, for a few sectors of limited area, two typical directions along which extension can be measured, but it is impossible to know whether or not these directions are the principal directions of strain. The first is a positive extension perpendicular to the mean orientation of the veins of the sector, the 'stretching direction'. The second is a negative extension parallel to the teeth of the stylotites and bisecting small-scale conjugate wrench faults, the 'shortening direction'. In Fig. 1, for each sector around the Meyrueis Fault, these directions are indicated out by centrifugal and centripetal arrows, respectively. It is noticeable that in no sector are these directions perpendicular one to the other. The stretching direction seems to be oriented E–W while the shortening direction has a trend of 020° or 030°, parallel to the Meyrueis Fault. Since the veins were formed before the other objects, as is indicated by field observations of stylolites and fractures, this may indicate that there has been a succession of stretching and shortening over a period of time, accompanied by a reorientation of the principal axes of finite strain which undergo a clockwise rotation.

As the position of veins is controlled by sedimentary anisotropy they are perpendicular to the layers (Hancock 1985). By adding together the thicknesses of veins observed at the surface of a layer, it is possible to determine how they bring about a change in its length. In the same way, the length of the teeth of the stylolites gives an idea of the shortening of a layer. Hence in some places, although the shape of the strain ellipsoid is unknown, the value of extension along the stretching and shortening directions may be established. The extension e is a ratio: $e = (L_1 - L_0)/L_0$, where L_0 and L_1 are the lengths of the object before and after deformation (Ramsay 1967). As the values are small, they are expressed in percent. Each circle in Fig. 1 is representative of a sector, and the measurements were taken in the following way.

(1) Positive extension (Fig. 2a) was measured across the veins. $L_1 - L_0$ is the sum of thicknesses of the different veins which can be observed on the top face of a sedimentary bedding, and L_0 is the sum of the widths of the different elements that have been cut off in this layer by the veins. To avoid, as far as possible, human error due to the operator, the measurement was taken along a string fixed tightly to the bedding, perpendicular to the veins; the string must cross at least 40 veins, which in this case means a distance of more than 5 m.

(2) Negative extension (Fig. 2b) was measured paral-

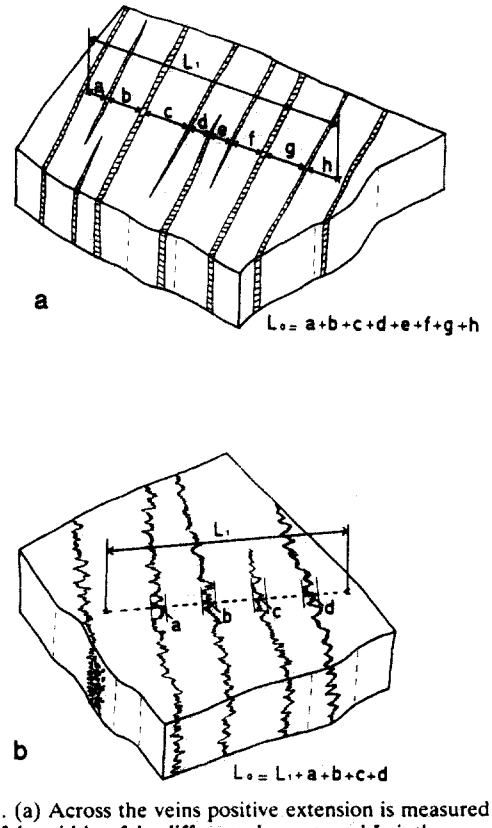

Fig. 2. (a) Across the veins positive extension is measured. L_0 is the sum of the widths of the different elements and L_1 is the present length. (b) Across the stylolites negative extension is measured, L_0 is the sum of L_1 (the present length) and the longest teeth of each stylolite.

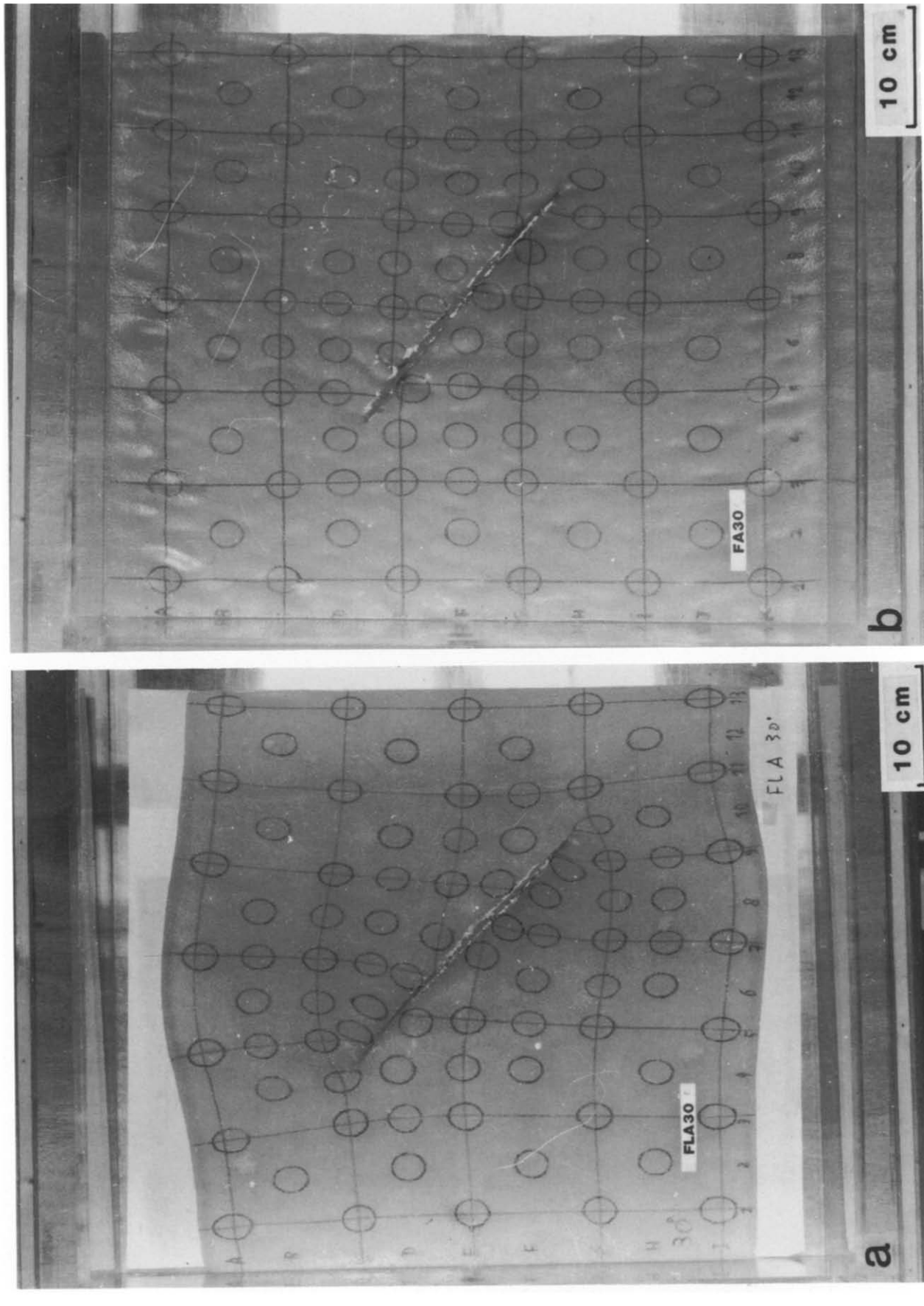

Fig. 3. Two types of experiments were carried out, one in which the layer did not fill the box and was free to expand (a), and another in which the layer completely filled the box (b). Obviously, heterogeneity of strain is more important in the first model. In these two experiments bulk shortening and the position of the fault before deformation are exactly the same.

lel to the 'teeth' of the stylolites. A string was tightly fixed perpendicular to the stylolites; its length is L_1, L_0 is then the sum of L_1 and the longest teeth of each stylolite. As the width of rock that disappeared in each stylolite because of solution may be greater than the longest teeth of the stylolite, L_0 may be underestimated (Stockdale 1922, Gratier 1984). The actual shortening may therefore be greater than indicated by the ratio given. To make sure of the reproducibility of the measurement the string must cross at least 40 stylolites, in a few metres of rock.

The results are presented in Fig. 1. For each sector the values of stretching and shortening are shown in front of the corresponding small arrows. Where no value is indicated, the measurement of extension was not possible with reasonable accuracy. It is noticeable that the intensity of strain, especially negative extension, is greatest in the north of the region shown in Fig. 1, where the fault disappears. Here it reaches about 5%.

Before presenting the experimental results, it may be useful to note the following main results of the field work: (a) the high degree of pressure solution; (b) stretching and shortening directions consistent with left-lateral movement along the fault, but which are not exactly synchronous and seem to indicate a rotation of the strain axes, with time; (c) concentration of horizontal compressive strain around the end of the fault; (d) the downfaulting of the western blocks; (e) small reverse faults around Florac, with compression towards 020°; and (f) intensity of the deformation which is about 5% and probably more.

Very diverse structures are arranged around the fault: reverse faults, normal movement and non-coaxial strain history. However, they are not randomly located and this suggests that their development and the left-lateral movement along the fault are linked together. To investigate this possibility, I made analogue models and focused on possible relations between deformation and displacement along a strike-slip fault.

RESULTS FROM ANALOGUE MODELS

The behaviour of a fault is a succession of brittle failures, at the limit of elasticity, which produce faulting and the accumulation of permanent strain over a long period. The propagation of cracks and fractures is a very rapid mechanism (Petit 1988); running cracks can accelerate to significant fractions of the velocity of sound (Atkinson 1987). In contrast, the growth of stylolites requires a long time (Gratier 1984) and the veins are progressively filled (Ramsay 1980). Hubbert (1937), who established the rules of similarity in analogue models, demonstrated that we could represent, in a few hours, the deformation of a geological structure that in reality required millions of years. However processes propagating at significant fractions of the velocity of sound in nature cannot be represented in experiments where time is accelerated by about 10^9. Thus, in a model it is not possible to represent all aspects of the behaviour of rocks, and we must choose between representing either the propagation of the fracture, or the accumulation of inelastic strain. This is a limitation imposed by the method.

As we were focusing on the study of strain around the fracture rather than the propagation of the fracture itself, we looked for a material able to represent time-dependent deformation. Elastic strain is then neglected; this is the kind of strain that develops during earthquakes (King & Vita-Finzi 1981) but probably never reaches 1%, whereas inelastic strain may exceed 10%. Thus neglecting elastic strains seems justified (Molnar 1983). Another result of elasticity is seismicity along the fault. But, as our experiment is unable to produce stick-slip, it represents only continuous displacement along an aseismic fault (Gratier & Gamond in press).

Since Rispoli (1981), it has been known that stylolites and veins can occur simultaneously and their relative positions agree with the reorientation of stresses around a fracture (Pollard & Segall 1987). The deformation of rocks by pressure solution is analogous to that of a viscous body (Laubscher 1975, Rutter 1976, Gratier 1984). The predominance of pressure solution around the Meyrueis Fault on Causse Méjean, therefore led me to select a viscous material for the experiments. In this case, I used a paraffin wax manufactured by MERCK, with a melting point of 46–48°C, and which is viscous at the temperature of the experiment (Mancktelow 1988).

In fact, the model represents the ductile behaviour around a fault. The period during which the deformation is produced is long enough to consider the displacement as being aseismic, with no propagation of the fault, and with the deformation being the result of viscous behaviour. The model is not scaled for gravity.

The models consist of a single layer of paraffin, 1.1 cm thick. A large number of layers would have produced an easy nucleation of folds, as shown by Biot (1961) and Ramberg (1964), but that would not have corresponded to my aim, which was the modelling of strain around a fault in a table-land context. The wax was placed in a rectangular box, 70 × 60 cm, made of Plexiglass (Odonne & Vialon 1987), and compressed by moving one of the shorter sides at a controlled rate of displacement throughout the experiment. Silicone grease (RHONE-POULENC, 70428), with silicone oil (RHODORSIL, 47 V 300) added to the proportion of three parts of grease to one part of oil, reduced friction along the walls and the bottom of the box. As the viscosities of paraffin and grease change with temperature, the experiments were performed in a thermostatically controlled airtight container at a temperature of 30°C. The viscosities of the materials are 3×10^5 Pa s for the paraffin wax and 10 Pa s for the grease. In each model a slit was made and filled with grease to allow displacement along itself. This represents a fracture likely to introduce heterogeneity in the deformation of the layer. To measure the strain at each point on the model, small circles were drawn in blue ink on the surface of the layer, 2.75 cm in diameter. Displacement of the wall was stopped every 5 cm, the finite strain on each circle, which

has now become an ellipse (Ramsay 1967), was measured, and I was therefore able to determine the deformation at each point and time of the experiment. Thus I know the strain history throughout the experiment.

I shall present in detail the results of two types of experiments. In one the angle between the fracture and the direction of compression is 30° (Fig. 3a) and the layer of wax does not fill the box. The dimensions of the layer are 70 × 45 cm, so the model is free to expand horizontally and vertically. In the other type of experiment the layer completely fills the box, which is likely to change the disposition of stresses at the boundaries of the model. Some other experiments, with the value of the fracture-compression angle varying from 15° to 45°, are only mentioned to complete the previous results or to specify some characteristic points.

At each stage of the experiment the position and geometry of each ellipse are measured; hence I can (a) draw displacement vectors, (b) draw principal axes of strain ellipses and (c) compare the geometry and position of each ellipse with that of the others or with its own geometry in a previous stage of deformation.

As each experiment is made up of four stages of deformation it is clear that only a computer is able to deal with the great amount of data. To avoid exhaustive but austere tables, results are presented as maps, where the centre of each ellipse is represented by a point or a symbol at the locus of the corresponding ellipse.

Model with horizontal stretching

By joining the initial and final positions of the centre of each ellipse we can draw the displacement vectors (Hobbs *et al.* 1976). These displacements are relative to a fixed origin, the same corner of the box in all the experiments, and they exhibit absolute displacement vectors (Fig. 4), from the undeformed state to stage 3. This vector, although precisely measurable, is not of much help to the geologist who is used to estimating displacements relative to a structural object. So, we can consider the centre of the fault as immobile during the deformation and draw relative displacement vectors (Ramsay & Huber 1983). Left-lateral displacement along the fracture is clear (Fig. 5) and the vectors located at the two tips of the fracture show its rotation in a clockwise direction. At the end of experiment this rotation reaches 14°. We obtain a different graph of relative displacement vectors if we subtract, graphically, the rotation of the fracture (Fig. 6). Then left-lateral displacement is obvious, 6.5 cm in the middle of the fracture, and at the end of experiment, vectors converge on the two areas where the thickness of the layer is greatest as a result of the concentration of matter.

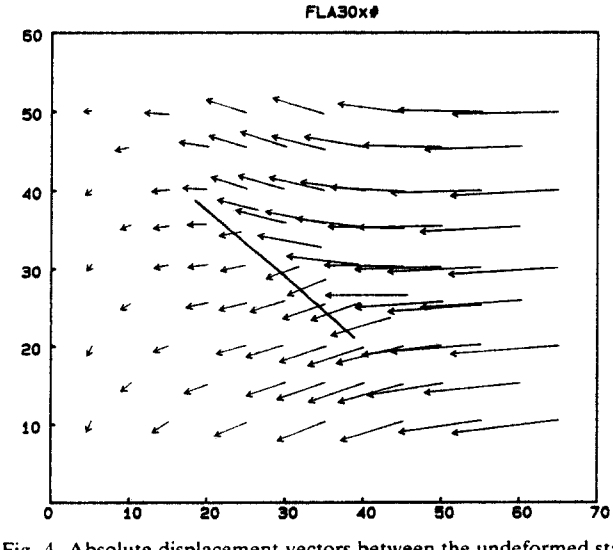

Fig. 4. Absolute displacement vectors between the undeformed state and stage 3 of the experiment where the layer does not fill the box. Scale in cm.

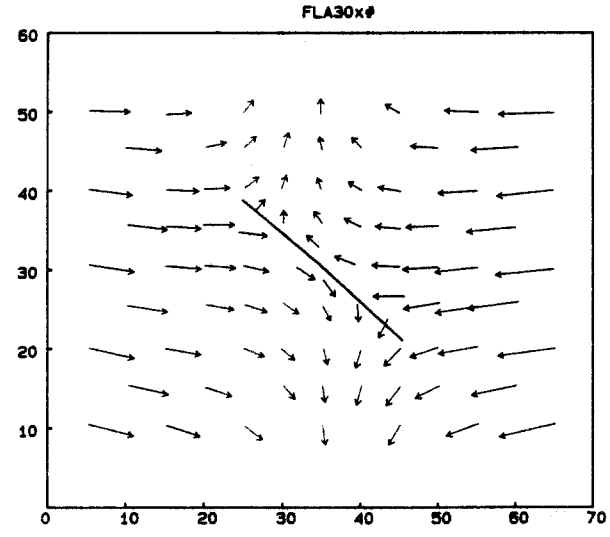

Fig. 5. Displacement vectors relative to the centre of the fracture. They exhibit left-lateral displacement along the fracture and the rotation of the fracture in a clockwise direction during the experiment. Scale in cm.

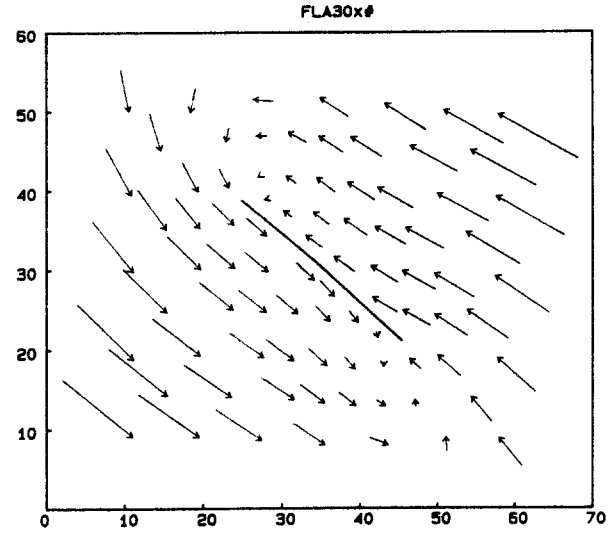

Fig. 6. Displacement vectors relative to the centre of the fracture, after removal of the rotation of the fracture. Displacement vectors converge on the two areas where the thickness of the layer is greatest at the end of experiment.

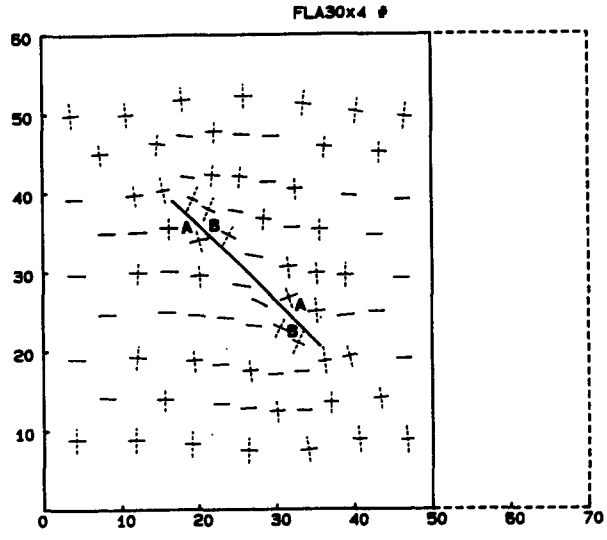

Fig. 7. Map of deformation at the end of the first experiment, where the layer does not fill the box and the fracture-compression angle is 30°. The short axes of the ellipses are represented by segments; if positive extension occurs along the long axes they are represented by dotted lines. The shortening is greater in sectors B than in sectors A. Dotted line is the initial position of the moving wall. Scale in cm.

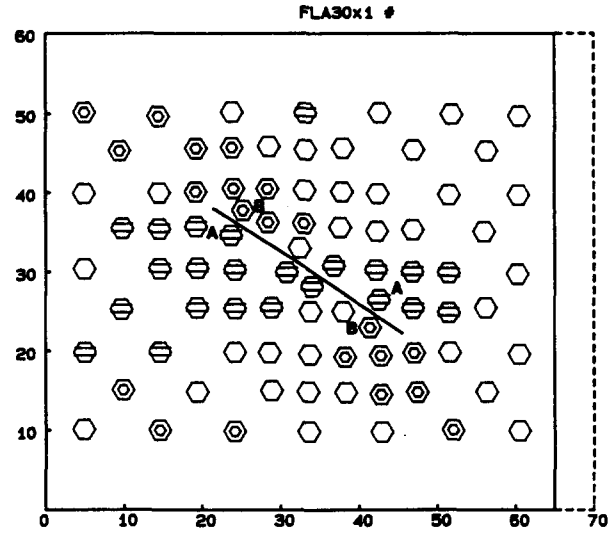

Fig. 8. Comparing of strains at equal distances from the moving wall, to eliminate strain heterogeneity associated with the wall. Horizontal shortening more than 10% greater than the mean is represented by concentric hexagons, more than 10% less than the mean is represented by hexagons with two parallel lines. Sectors A are protected areas, sectors B are areas of high shortening. These sectors are well defined early in the deformation history, after 5 cm of displacement of the wall in the experiment where the layer does not fill the box.

Figure 7 shows the map of deformation at the end of the experiment, when displacement of the short side of the box reaches 20 cm. The short axes of the ellipses are represented by segments; the long axes are shown with dotted lines if the extension e along them reaches more tham +4%. If we assume that during deformation the volume of paraffin does not change, the change in area of each ellipse is balanced by the thickening of the layer, and the geometry of finite strain ellipsoids is known. Using the Flinn diagram in Ramsay (1967, p.136), we can define these ellipsoids around the fracture: $k = 0.16$ in sectors A, $k = 0.4$ in sectors B, always of the flattened type. The finite strain ellipses vary in orientation around the fracture; in sectors A short axes tend to be at high angles to the fault, in sectors B they tend to be at low angles, which agrees with Anderson (1951).

As a unilateral compression is acting on the model, the strain is greater close to the moving wall than in the rest of the model. This is superimposed on the heterogeneous strain introduced by the fracture. For the best understanding of the latter we have to eliminate the influence of the moving wall. To do this, all ellipses located at equal distances from the moving wall are compared. A mean value of the length of the short axes of finite strain ellipses in each group is calculated, and each ellipse is then checked with the mean of its group (Fig. 8). If the shortening differs by more than 10% from the mean, a superimposed symbol is shown on the hexagons that represent the location of strain measurements. Concentric hexagons are shown if the shortening is greater than the mean, and parallel lines if less. Protected areas (domains A) and high strained areas (domains B) appear at the very beginning of deformation; these are clearly visible after only 5 cm displacement of the wall. This agrees with other experimental results (Wang *et al.* 1987).

To understand how the variations in strain orientation shown in Fig. 7 develop, we can compare deformation of the model at successive stages. On the same diagram the short axes of two successive stages are superimposed. In Fig. 9, the axes of stage 1 and stage 2 are superimposed, and it clearly appears that in some places a difference of at least 15° exists between the successive orientations of finite strain ellipses, while the rotation of the fracture is only 4° between stages 1 and 2. This represents a non-coaxial strain history around the fracture. At the end of deformation, between stages 3 and 4, rotation of the ellipses is weaker (Fig. 10). To define the sense of this rotation between stages 1 and 2, Fig. 11 represents each ellipse by a circle. If the rotation exceeds 3°, the circles are replaced by clockwise and anticlockwise vectors.

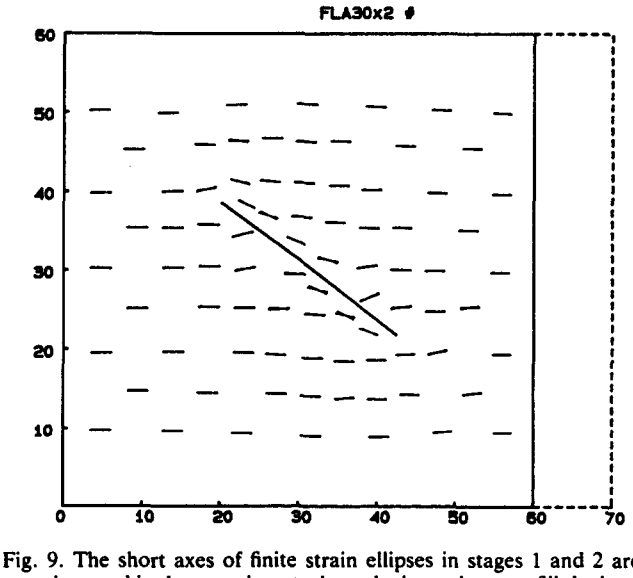

Fig. 9. The short axes of finite strain ellipses in stages 1 and 2 are superimposed in the experiment where the layer does not fill the box. In some places the two axes are not exactly parallel which reveals a non-coaxial strain history.

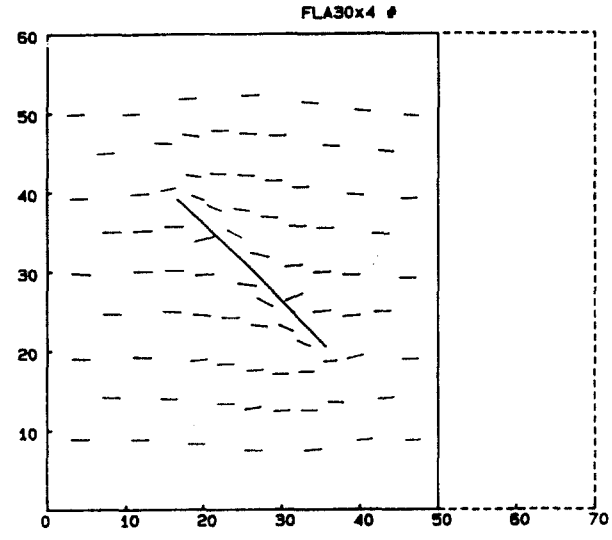

Fig. 10. At the end of the experiment (see Fig. 9 for the beginning) the short axes of the last two stages are superimposed. There is no rotation of the principal axes of strain. Scale in cm.

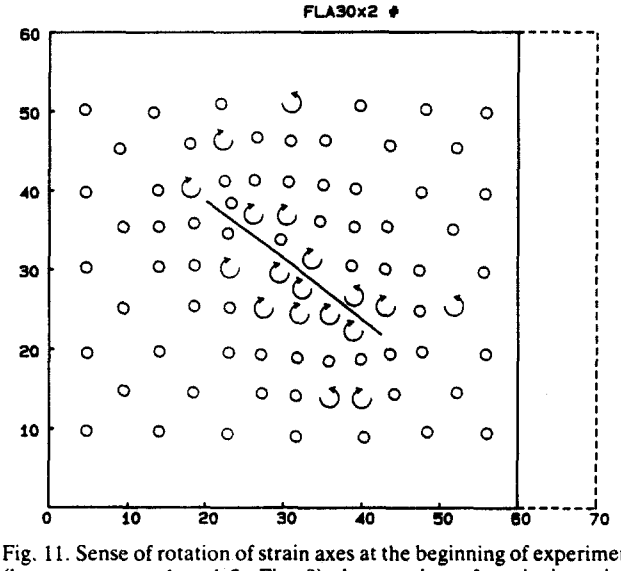

Fig. 11. Sense of rotation of strain axes at the beginning of experiment (between stages 1 and 2, Fig. 9) the rotation of strain is mainly clockwise.

During this second step, from stage 1 to stage 2, it is mainly clockwise rotation that appears around the fracture. The behaviour of the model during this step is especially interesting because the intensity of strain corresponds to that observed around the Meyrueis Fault.

Data from additional models

To study the influence of a parameter, it must be changed from one model to the next. Then any change in the deformation of the model may be linked to this parameter, and only this one. I shall consider first the influence of the disposition of the principal stress axes in relation to the boundaries of the model and the influence of the orientation of the fracture within the model.

In the second type of experiments the paraffin layer

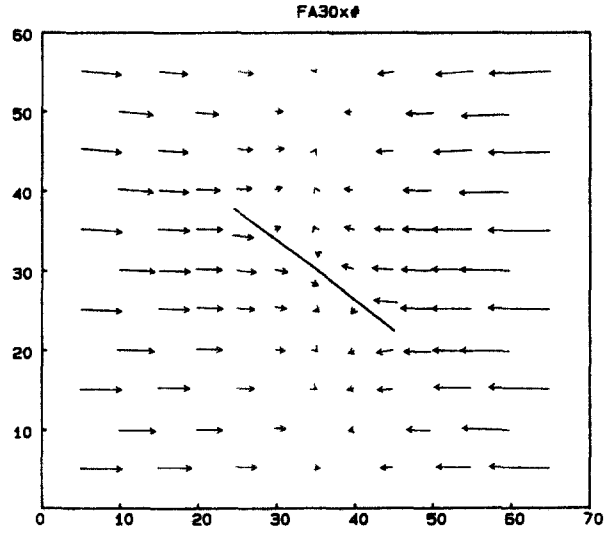

Fig. 12. Displacement vectors relative to the centre of the fracture, in the experiment where the layer completely fills the box, between the undeformed state and stage 3. They exhibit small left-lateral displacement along the fracture, and a small rotation of the fracture in a clockwise direction during the experiment. In Fig. 5 where the layer does not fill the box, displacement and rotation are obviously greater.

fills the Plexiglass box (Fig. 3b), the angle between the fracture and the compression being always 30° at the beginning of the deformation. The boundaries of the model were constrained along the long sides of the box, parallel to the compression direction, and this may be compared to an intermediate principal stress. In the vertical direction the weight of the layer only exerts extremely low stresses. Such a disposition does not ease displacement along the fracture, but a small displacement is observed of 2.8 cm, in a left-lateral direction (Fig. 12) and a small clockwise rotation of the fracture, 9°. Compare with Fig. 5.

The deformation map shows the change in orientation of each finite strain ellipse around the fracture (Fig. 13,

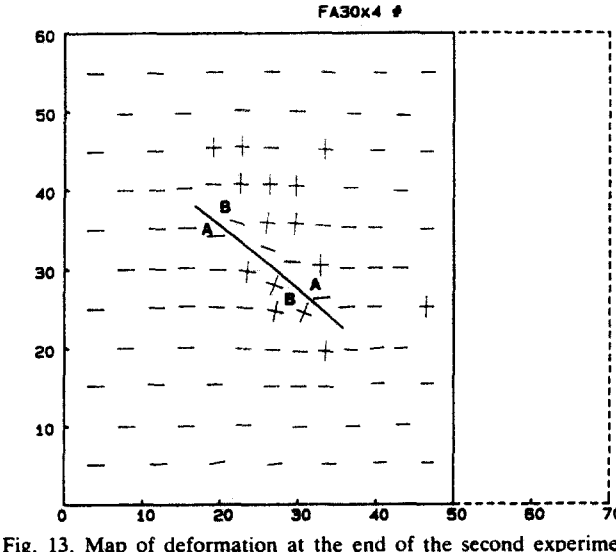

Fig. 13. Map of deformation at the end of the second experiment where the layer fills the box. The short axes of the ellipses are represented by lines, and if negative extension has occurred along the long axes they are also shown (in sectors B where thickening of the layer is greater). In contrast to Fig. 7 (first experiment), no horizontal stretching occurs but the shortening is always greater in sectors B than in sectors A. Scale in cm.

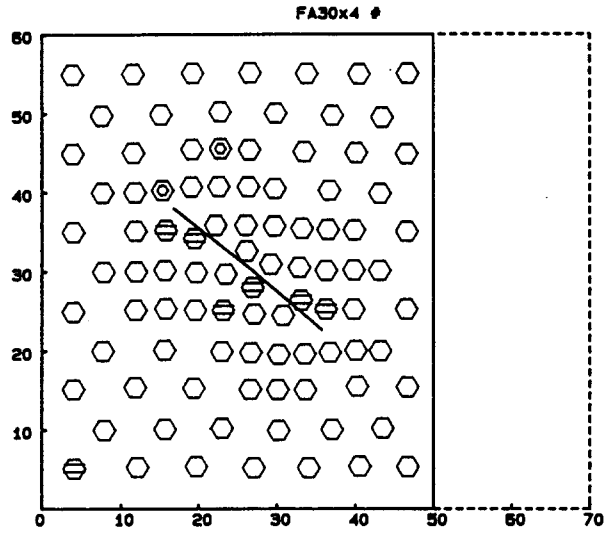

Fig. 14. Experiment of the second type. As in Fig. 8, strain heterogeneity associated with the moving wall has been eliminated. Shortened ellipses are represented by concentric hexagons, and protected ellipses are represented by hexagons with two parallel lines. Even at the end of experiment (stage 4), protected areas do not appear as clearly as in the first stage of deformation of the model with free sides.

compared with Fig. 7). The long axes of the ellipses are never stretched, but they are sometimes shortened and then appear as a line. Obviously, corresponding ellipsoids are constricted and their shape is defined as before with the Flinn diagram: $k = 1.25$ in sectors A, $k = 1.75$ in sectors B. The heterogeneity of strain is not so clearly seen as in the previous model, protected areas seem to appear only at the end of the deformation (Fig. 14). Rotation of the ellipses takes place around the fracture only. At the end of the experiment we can observe limited, but clearly defined areas at the tips of the fracture: sectors A which exhibit anticlockwise rotation and sectors B, clockwise rotation (Fig. 15).

To summarize the different evolutions of these two models, Fig. 16 represents the shapes and orientations of finite strain ellipsoids in sectors A and B, at the end of the deformation. The importance of the heterogeneity introduced in the model by the fracture is clear when the model is free to expand (Fig. 16a), and it is lessened when the boundaries are fixed (Fig. 16b). Hence the heterogeneity seems to be linked to the amount of displacement along the fracture.

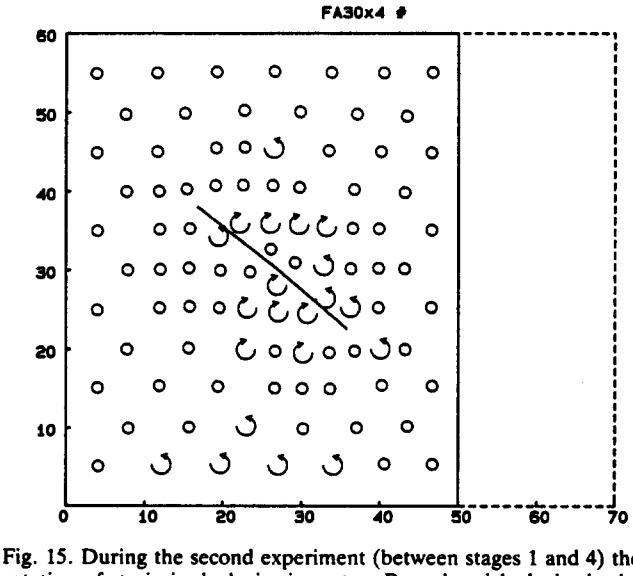

Fig. 15. During the second experiment (between stages 1 and 4) the rotation of strain is clockwise in sectors B, and anticlockwise in the sectors A. This rotation of strain is well expressed at the end of the experiment only.

In another set of experiments the value of the fracture-compression angle is 15° or 45°. In both cases the differences observed in the evolution of the models, whether with fixed lateral boundaries or not, confirm the previous results. This was in agreement with the Coulomb theory (1776) which states that displacement along a fracture occurs more easily when the fracture compression angle is between 30° and 45° (see also Chinnery 1966). So, in models where this angle is 15°, deformation with a low heterogeneity is observed and disturbance introduced by the fracture is not widespread. Results from models where the angle is 45° are close to those of 30° models, however, the angle between the fracture and the short axis of each ellipse is always greater than in the 30° models. At the end of the experiment evolution is noticeably different: ellipses rotate to align more closely with the compression direction; the fracture, with a clockwise rotation of 14°, leaves the position where left-lateral displacement is easy, and heterogeneity is reduced and strain ellipses tend to become parallel once again.

CONCLUSION FROM THE MODELS

The main results of the experiments may be summarized as follows.

(1) Left-lateral displacement along the fracture causes reorientation of the principal strain axes.

(2) As this reorientation appears progressively, strain history is clearly non-coaxial around the fracture, especially at the beginning of the deformation where clockwise rotations arise.

(3) Domains where shortening is intense, and others where it is very slight become more individualized as the deformation proceeds, and the positions of these domains are symmetrical with respect to the fault.

(4) Heterogeneity of strain is linked to the amount of the displacement along the fracture, that is to say: (a) to the possibility for the layer to expand in its horizontal plane, (b) to the fracture-compression angle.

DISCUSSION

Deformation around the Meyrueis Fault involves E–W stretching, and a shortening which may exceed 5%, trending close to the fault direction, that is to say 030°. This and the important left-lateral displacement along the fault, lead us to retain, as a reasonable analogy, the model with free sides.

The thickening of domains B, where the relative displacement vectors converge as a result of matter

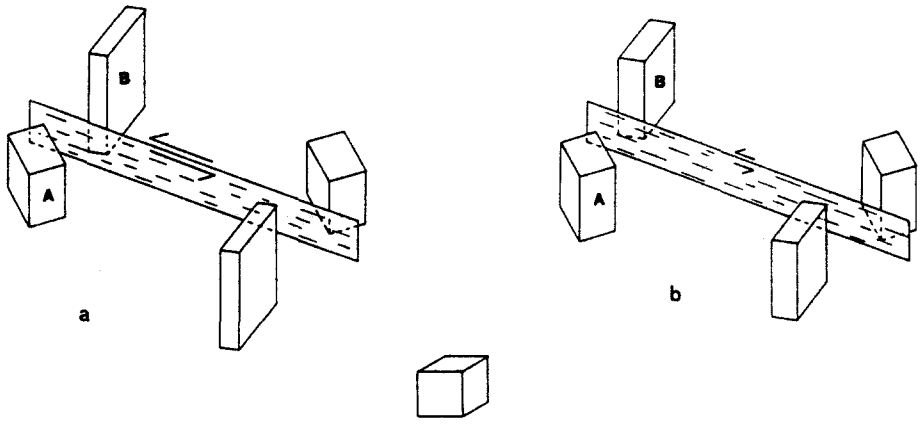

Fig. 16. Comparison of shapes and orientations of finite strain ellipsoids of the two models, here, at the end of each experiment. Each ellipsoid is represented by a parallelepiped derived from a cube representing the undeformed state. (a) Model with free sides, the heterogeneity of strain is great. (b) Model which fills the box, the heterogeneity of strain is reduced. Here, the heterogeneity seems to be related to the size of displacement along the fracture.

concentration, seems to correspond, in the field example, to the small reverse faults around Florac, and the lowering of the western blocks corresponds to domains A. This agrees with the models of Rodgers & Chinnery (1973) and Sibson (1985), where on one side of the fault there is an area with positive vertical movement, and on the other side negative movement. The relative positions of these domains confirm the important left lateral movement along the Meyrueis Fault.

The rotation of the deformation in a clockwise direction during stage 2 of the experiment can be compared to the succession of stretching (N–S veins) and shortening (teeth of stylolites at 030°) around the fault. However, these directions (of the veins and teeth of stylolites), which correspond to intermediate stages of deformation, are not equivalent to the principal directions of strain as inferred from the models. Nevertheless, as the veins were formed first, this suggests, by analogy with the models, that the strain history around the Meyrueis Fault is non-coaxial and that the strain axes have rotated progressively in a clockwise direction.

The answer to the question suggested above is thus that a single lateral movement along a pre-existing fracture is able to produce, in well defined domains, reverse faults, normal movements and a non-coaxial strain history.

One conclusion that we may draw from this study is that a fracture locally disturbs the disposition of stresses and deformation. Strain history, around the fault, is clearly non-coaxial, and this deformation rotation is a function of the following factors.

(1) The freedom of the boundaries of the layer, which may also be expressed as the horizontal position, or otherwise, of principal intermediate stress. When the boundaries are free, unrestricted displacement occurs easily along the fracture and heterogeneous strain, with major rotations, is possible.

(2) The angle between the fracture and the direction of compression. When this angle is between 30° and 45° displacement is possible, and rotations occur.

(3) The intensity of the deformation. A bulk shortening exceeding 30% would destroy heterogeneity of strain, finite strain ellipses beginning to be more and more parallel. In the early stages of deformation the heterogeneity appears. As the experiment progresses the fracture rotates and when the fracture-compression angle exceeds 45°, displacement is reduced and the heterogeneity disappears.

Acknowledgements — I thank the Société Nationale Elf Aquitaine (Production) who has financed this research programme and has permitted publication. I thank Professor P. Vialon for his substantial help and support throughout this work, and X. Allemandou for help during field work. Special thanks to the reviewers, J.-F. Gammond and J. Watterson, for constructive criticisms and to J. P. Platt who improved the text.

REFERENCES

Anderson, E. M. 1951. *The Dynamics of Faulting*. Oliver & Boyd, Edinburgh.

Arthaud, F. & Mattauer, M. 1969. Exemples de stylolites d'origine tectonique dans le Languedoc, leurs relations avec la tectonique cassante. *Bull. Soc. Géol. Fr.* 7, 738–744.

Atkinson, B. K. 1987. *Fracture Mechanics of Rock*. Academic Press, New York.

Biot, M. A. 1961. Theory of folding of stratified viscoelastic media and its implications in tectonics and orogenesis. *Bull. geol. Soc. Am.* 72, 1595–1620.

Chinnery, M. A. 1961. The deformation of the ground around surface faults. *Bull. seism. Soc. Am.* 51, 355–372.

Chinnery, M. A. 1963. The stress changes that accompany strike-slip faulting. *Bull. seism. Soc. Am.* 53, 921–932.

Chinnery, M. A. 1966. Secondary faulting I. Theoretical aspects. *Can. J. Earth Sci.* 3, 163–174.

Chiron, J. C. 1980. Introduction à la Carte Tectonique de la France. *Mém. Bur. Rech. géol. & Minières Orléans.*

Coulomb, C. A. 1776. Essai sur une application des règles des maximis et minimis à quelques problèmes de statique relatifs à l'architecture. *Mem. Acad. Sci. Paris*, 7.

de Charpal, O & Trémolières, P. 1974. Un exemple de tectonique de plate-forme: les Causses Majeurs. *Revue Institut Fr. Pétrole* 29, 641–659.

Freund, R. 1965. A model of the structural development of Israel and adjacent areas since upper Cretaceous times. *Geol. Mag.* 102, 189–205.

Freund, R. 1970. Rotation of strike slip faults in Sistan, Southeast Iran. *J. Geol.* 78, 188–200.

Gamond, J. F. 1983. Displacement features associated with fault zones: a comparison between observed examples and experimental models. *J. Struct. Geol.* **5**, 33–45.

Gèze, B. 1977. Geological Map of Meyrueis (1/50 000). *Bur. Rech. geol & Minières. Orlèans.*

Gratier, J. P. 1984. La Deformation des Roches par Dissolution-Cristallisation. Unpublished thesis, University of Grenoble.

Gratier, J.-P. & Gammond, J.-F. In press. Transition between seismic and aseismic deformation in the upper crust. *Spec. Publs geol. Soc. Lond.*

Hancock, P. L. 1985. Brittle microtectonics: principles and practice. *J. Struct. Geol.* **7**, 437–457.

Harding, T. P. 1974. Petroleum traps associated with wrench faults. *Bull. Am. Ass. Petrol. Geol.* **58**, 1290–1304.

Hobbs, B. E., Means, W. D. & Williams, P. F. 1976. *An Outline of Structural Geology.* Wiley, New York.

Hubbert, K. 1937. Theory of scale models as applied to the study of geologic structures. *Bull. geol. Soc. Am.* **48**, 1459–1520.

King, G. C. P. & Vita-Finzi, C. 1981. Active folding in the Algerian earthquake of 10 October 1980. *Nature* **292**, 22–26.

Laubscher, H. P. 1975. Viscous components in Jura folding. *Tectonophysics* **27**, 239–254.

McKenzie, D. & Jackson, J. 1983. The relationship between strain rates, crustal thickening, paleomagnetism, finite strain and fault movements within a deforming zone. *Earth Planet. Sci. Lett.* **65**, 182–202.

Mancktelow, N. 1988. The rheology of paraffin wax and its usefulness as an analogue for rocks. *Bull. geol. Inst. Univ. Uppsala* **14**, 181–193.

Means, W. D. 1987. A newly recognized type of slickenside striation. *J. Struct. Geol.* **9**, 585–590.

Molnar, P. 1983. Average regional strain due to slip on numerous faults of different orientations. *J. geophys. Res.* **88**, 6430–6432.

Moody, J. D. & Hill, M. J. 1956. Wrench-fault tectonics. *Bull geol. Soc. Am.* **67**, 1207–1246.

Moody, J. D. 1973. Petroleum exploration aspects of wrench-fault tectonics. *Bull. Am. Ass. Petrol Geol.* **57**, 449–476.

Naylor, M. A., Mandl, G. & Sijpesteijn, C. H. K. 1986. Fault geometries in basement-induced wrench faulting under different initial stress states. *J. Struct. Geol.* **8**, 737–752.

Odonne, F. & Vialon, P. 1987. Hinge migration as a mechanism of superimposed folding, *J. Struct. Geol.* **9**, 835–844.

Oertel, G. 1965. The mechanism of faulting in clay experiment. *Tectonophysics*, **2**, 343–393.

Petit, J.-P. 1988. Normal stress dependent rupture morphology in direct shear tests on sandstone with applications to some natural fault surface features. *Int. J. Rock Mech. Min. Sci. & Geomech. Abs.* **25**, 411–419.

Pollard, D. D. & Segall, P. 1987. Theoretical displacements and stresses near fractures in rock: with applications to faults, joints, veins, dikes, and solution surfaces. In: *Fracture Mechanics of Rock.* Academic Press, New York.

Ramberg, H. 1964. Selective buckling of composite layers with contrasted rheological properties, a theory for simultaneous formation of several orders of folds. *Tectonophysics* **1**, 307–341.

Ramsay, J. G. 1967. *Folding and Fracturing of Rocks.* McGraw-Hill, New York.

Ramsay, J. G. 1980. The crack–seal mechanism of rock deformation. *Nature* **284**, 135–139.

Ramsay, J. G. & Huber, M. I. 1983. *The Techniques of Modern Structural Geology, Volume 1: Strain Analysis.* Academic Press, London.

Rispoli, R. 1981. Stress fields about strike-slip faults inferred from stylolites and tension gashes. *Tectonophysics*, **75**, T29–T36.

Rodgers, D. A. & Chinnery, M. A. 1973. Stress accumulation in the Transverse Ranges, Southern California. *Stanford University Publs* **XIII**, 70–79.

Rutter, E. H. 1976. The kinetic of rock deformation by pressure-solution. *Phil. Trans. R. Soc. Lond.* **A283**, 43–54.

Sanderson, D. J. & Marchini, W. R. D. 1984. Transpression. *J. Struct. Geol.* **6**, 449–458.

Segall, P. & Pollard, D. D. 1980. Mechanics of discontinuous faults. *J. geophys. Res.* **85**, 4337–4350.

Sibson, R. 1985. Stopping of earthquake ruptures at dilational fault jogs. *Nature* **316**, 248–251.

Stockdale, P. B. 1922. Stylolites, their nature and origin. Unpublished thesis, University of Indiana.

Wang, R., Zhao, Y., Chen, Y., Yan, H., Yin, Y., Yao, C. & Zhang, H. 1987. Experimental and finite element simulation of X-type shear fractures from a crack in marble. *Tectonophysics* **144**, 141–150.

White, S. H., Bretan, P. G. & Rutter, E. H. 1986. Fault-zone reactivation: kinematics and mechanisms. *Phil. Trans. R. Soc. Lond.* **A317**, 81–97.

Wilcox, R. E., Harding, T. P. & Seely, D. R. 1973. Basic wrench tectonics. *Bull. Am. Ass. Petrol. Geol.* **57**, 74–96.

Xiaohan, L. 1983. Perturbation de contraintes liées aux structures cassantes dans les calcaires fins du Languedoc, observations et simulations mathématiques. Unpublished thesis, University of Montpellier.